# DESIGN OF SOLID-STATE IMAGING ARRAYS

Marvin H. White

Lehigh University
Sherman Fairchild Center
Bethlehem, PA.

U.S.A.

ABSTRACT. In this chapter the various factors which influence the design of solid-state imaging arrays will be discussed. Responsivity, spectral response, resolution, noise, streaking, dynamic range, etc, will be treated with the concept of a figure-of-merit based upon the product of S/N and M.T.F. (eff.).

## 1. SPECTRAL RESPONSE $R_\lambda$

A sensor, such as a silicon photodiode, constructed in an intrinsic semiconductor has a spectral response given as,

$$R_\lambda = \frac{e\,\eta(\lambda)}{hc/\lambda}\, U(\lambda_G - \lambda) \tag{1}$$

where $\lambda_G = hc/E_G$ is the cut-off wavelength for an intrinsic band gap $E_G$ and $\eta(\lambda)$ is the effective quantum efficiency. $U(\lambda_G - \lambda)$ is a unit step function defined as,

$$U(\lambda_G - \lambda) = 1 \qquad \lambda \leq \lambda_G$$

$$= 0 \qquad \lambda > \lambda_G$$

Figure 1 illustrates the theoretical and experimental spectral responses for a silicon photodiode. The departure at short wavelengths ($\lambda < 400$ nm) is attributed to surface trapping of the generated minority carriers, while the long wavelength fall-off is due to bulk trapping ($\lambda > 800$ nm). In the wavelength region

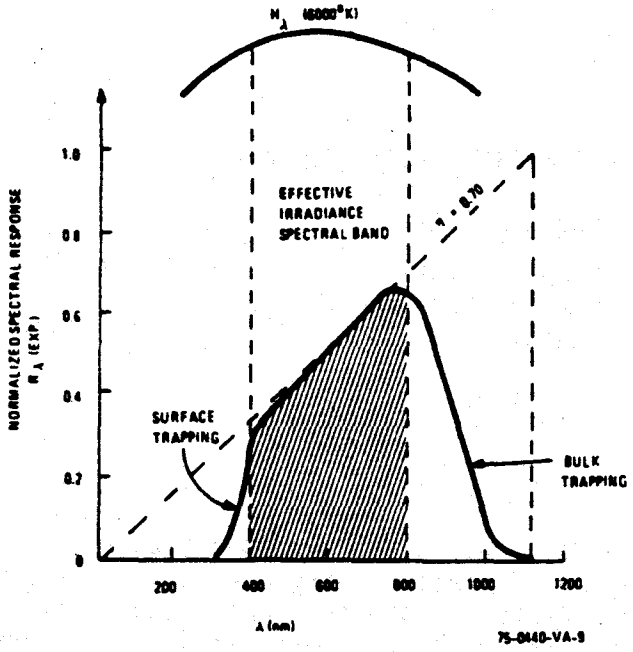


Figure 1. Spectral Response and Responsivity for a Silicon Photodiode (Dotted Curve is Ideal Spectral Response, Solid Curve is Experimental Spectral Response)

400 nm $\leq \lambda \leq$ 800 nm, the silicon photodiode approximates an ideal photon detector with a constant effective quantum efficiency determined by the silicon reflectivity,

$$\eta \simeq 1 - \left(\frac{N_{si} - N_{air}}{N_{si} + N_{air}}\right)^2 = 1 - \left(\frac{3.45-1}{3.45+1}\right)^2 = 0.70 \qquad (2)$$

where we have neglected the imaginary part of the index of refraction caused by absorption of radiation. The units of spectral response are amperes/watt or current density output per irradiance input.

$$R_\lambda = \frac{J_\lambda}{H_\lambda} \left(\frac{A/m^2}{W/m^2}\right) \qquad (3)$$

## 1.1 Responsivity Formulation R

The responsivity of a photosensor may be defined with respect to a spectral band $(\lambda_2, \lambda_1)$ as follows.[1]

$$R \equiv \frac{I}{H(\text{eff.})} = \frac{\int_{\lambda_1}^{\lambda_2} R_\lambda H_\lambda d_\lambda}{\int_{\lambda_1}^{\lambda_2} H_\lambda d_\lambda} \left(\frac{A}{W/m^2}\right) \tag{4}$$

where H(eff.) is an effective irradiance over the spectral band $(\lambda_2, \lambda_1)$ and $H_\lambda$ is an ideal blackbody irradiance given as

$$H_\lambda = \frac{2\pi c^2 h}{\lambda^5 \left(e^{hc/\lambda k T_s} - 1\right)} \left(\frac{W}{m^2 \cdot \mu m}\right) \tag{5}$$

If we assume the effective quantum efficiency $\eta$ is constant or slowly varying over the spectral band of interest, then we can write equation (4) as

$$R = \frac{e\eta}{kT_s} \frac{\int_{X_1}^{X_2} X^2 e^{-X} dx}{\int_{X_1}^{X_2} X^3 e^{-X} dx} \tag{6}$$

where $X = hc/\lambda kT_s >> 1$ and $T_s$ the specified source temperature. For a blackbody source temperature of $T_s = 6000°K$ (i.e. the "sun") and $\lambda_1 = 400$ nm, $\lambda_2 = 800$ nm, we can write for the silicon photodiode,

$$R \begin{pmatrix} \lambda_1 = 400 \text{ nm}, \lambda_2 = 800 \text{ nm} \\ \eta = 0.70 \quad T_s = 6000°K \end{pmatrix} = 0.33 \frac{A}{W} \tag{7}$$

where the watts are W - 6000°K effective within the 400 nm to 800 nm spectral band. For example, consider a silicon photodiode with area A = 15 $\mu$m x 20 $\mu$m. The detector responsivity may be written as,

$$R_D = RA = \frac{0.0984pA}{mW/m^2} \left(\frac{616e^-}{\mu J/m^2}\right) \tag{8}$$

with an alternate method of $e^-$ (electrons) per effective exposure density E (eff.) in $\mu J/m^2$.

## 1.2 Measurement of Effective Irradiance H (eff.)

The responsivity, given by equation (4), is defined in terms of a specified blackbody source (e.g. $T_S$ = 6000°K) which we shall designate the "spec" source. In practice the actual "test" source may be quite different (e.g. $T_T$ = 2856°K). The irradiance and spectral response of the "test" source are measured with a standard diode and narrow band filters (or a monochromator) and the current output of the detector is equated to the current output of a hypothetical "spec" source irradiated detector. Thus, we may write

$$\begin{aligned} I_{TEST} &= R_\lambda(max)\, H_\lambda(max)_{TEST} \int_{200}^{1200} \bar{R}_\lambda\, \bar{H}_\lambda\,(TEST)\, d\lambda \\ I_{SPEC.} &= R_\lambda(max)\, H_\lambda(max)_{SPEC.} \int_{400}^{800} \bar{R}_\lambda \bar{H}_\lambda(SPEC.)\, d\lambda \end{aligned} \tag{9}$$

where $\bar{R}_\lambda$ and $\bar{H}_\lambda$ are normalized quantities. If we equate $I_{SPEC.} = I_{TEST}$ and use the $T_S$ = 6000°K radiation integrals, then we have

$$H(eff.) = \int_{400}^{800} H_\lambda(SPEC.)d\lambda = 343\, H_\lambda(max)_{TEST} \frac{\int_{200}^{1200} \bar{R}_\lambda \bar{H}_\lambda(TEST)d\lambda}{\int_{400}^{800} \bar{R}_\lambda \bar{H}_\lambda(SPEC.)\, d\lambda} \left(\frac{mW}{m^2}\right) \tag{10}$$

We should notice the integration limits on the "test" source (i.e. $\lambda_1$ = 200 nm, $\lambda_2$ = 1200 nm) are determined by the cut-off imposed by the sensor spectral response $R_\lambda$. For example, the photodiode and CCD detectors shown in figure 2 had effective irradiance levels of

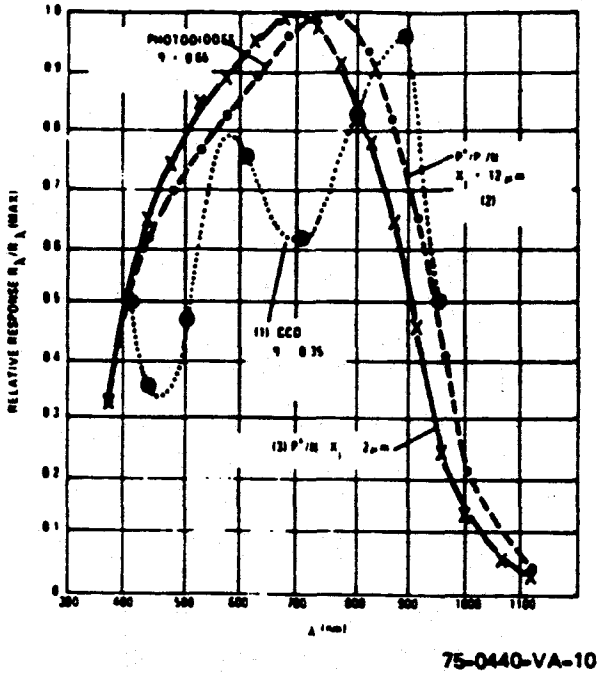


Figure 2. Phototransistor and CCD Relative Spectral Response Curves

$$H(\text{eff.})_{\text{Photodiode}} = 0.639 \text{ mW/m}^2$$

$$H(\text{eff.})_{\text{CCD}} = 0.762 \text{ mW/m}^2$$

for a particular setting of the "test" source lamp current. The above example illustrates the influence of the spectral response of the detector on the determination of effective irradiance levels. In practice, the signal-to-noise and dynamic range of the detectors are measured by attenuation of the effective irradiance level with neutral density filters.

## 1.3 Radiometric and Photometric Characteristics

In the preceding sections the sensor was described in terms of radiometric units (e.g. watts) and the watt was defined as the effective power from a 6000°K blackbody over the 400-nm to 800-nm spectral band. Thus, it is important to define the temperature of the source and the spectral band of interest in order to describe the type of "watt". The standard radiant flux for the human eye is the foot-candle (lumens/ft$^2$) or meter-candle (lumens/m$^2$) and it is a measure of stimulation of the human perceptual system. When the human eye is used as a standard the relative spectral response (i.e. standard "observer") curve of figure 3 is the spectral weighting function $\bar{R}_\lambda$. To describe an

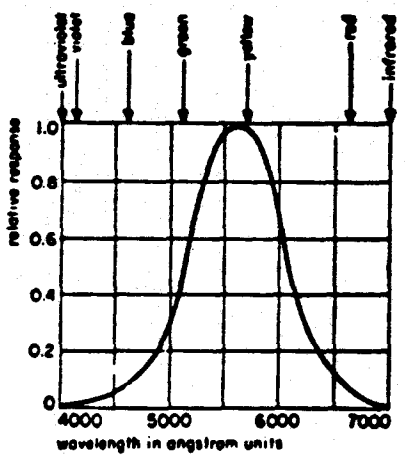


75-0440-VA-11

Figure 3. Spectral Response (Relative) of the Human "Eye"

electro-optical device such as silicon in terms of $1m/m^2$ is somewhat misleading since the sensor has a spectral response outside the visible range. Perhaps the best procedure is to describe the sensor response in radiometric units (A/W) and then divide this response by the luminosity of the test source (lm/W). The relative spectral response of the human "eye" is shown in figure 3 and with the standard definition of $60\pi lm/cm^2$ as the total luminance from a 2042°K platinum source falling within the passband of the eye we can write

$$R_\lambda(max)_{EYE} = \frac{60\pi \times 10^4}{\int_0^\infty \bar{R}_\lambda(EYE)\, H_\lambda(2042°K)d\lambda} \tag{11}$$

The spectral luminance from a test source $T_T$ may be written as

$$F = 680 \int_0^\infty \bar{R}_\lambda(EYE) H_\lambda(T_T)d\lambda \tag{12}$$

and the luminosity becomes

$$K = \frac{F}{\int_0^\infty f(\lambda)H_\lambda(T_T)d\lambda} \tag{13}$$

where $f(\lambda)$ is the filter characteristic of the source. K, the luminosity coefficient, is the ability of the test source to convert watts (radiant power) to lumens (luminescent power). In general, $f(\lambda)$ cuts off beyond 2.7 $\mu$m for most glasses and the upper limit of the integral is determined by the glass transmission. Thus, the number of effective blackbody watts is reduced by the glass envelope surrounding the test source. If we consider the so-called tungsten "lumen" from a T = 2856°K source, then equation (13) becomes

$$K\begin{pmatrix}\lambda_c = 2.7\ \mu m \\ T_T = 2856°K\end{pmatrix} = 20\ \frac{lm}{W} \tag{14}$$

The sensitivity of the sensor is calculated by dividing equations (6) and (13). In the case of the photodiode we have,

$$S = \frac{R}{K} = 0.33/20 = 16.5\ \frac{mA}{lm} \tag{15}$$

The ideal luminosity K = 16.5 lm/W is obtained for radiation over all wavelengths. Figure 4 illustrates the luminous efficiency and luminosity of a blackbody as a function of absolute temperature.

The key point in the understanding of photometric units is that a lumen represents the amount of radiant power incident on the sensor when the luminous flux at the sensor is one lumen. The use of lumens does not provide the user any information with respect to radiant sensitivity and the specification of performance must consider the spectral distribution of the incident power. Figures 5 and 6 illustrate the natural illuminance levels on the surface of the earth and the range of these levels. The conversion of these photometric units into radiometric units requires a knowledge of the spectral distribution of the radiation. For example, if we consider the sun ($T_s$ = 6000°K) and define the integration limits from $\lambda_1$ = 400 nm to $\lambda_2$ = 800 nm, then the luminosity becomes

$$K\begin{pmatrix}\lambda_1 = 400\ nm,\ \lambda_2 = 800\ nm \\ T_s = 6000°K\end{pmatrix} \simeq \frac{200\ lm}{W}$$

whereas, integration over all wavelengths yields 90 lm/W as seen from figure 4.

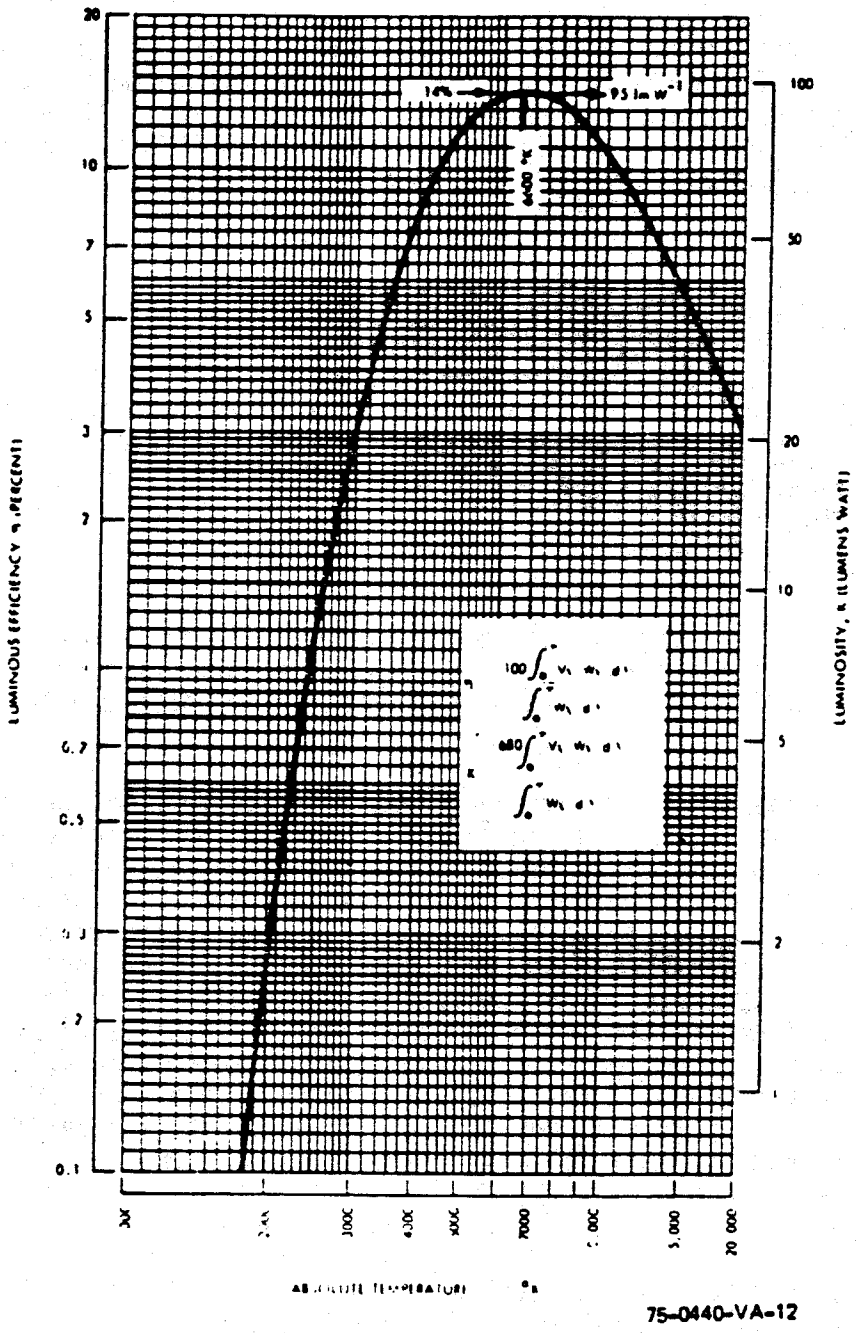


Figure 4. Luminous Efficiency $\eta$ and Luminosity K of Blackbody as a Function of its Absolute Temperature where $W_\lambda$ is the Spectral Radiant Emittance of the Blackbody and $V_\lambda$ is the Relative Spectral Response of the Average Human Eye.[3]

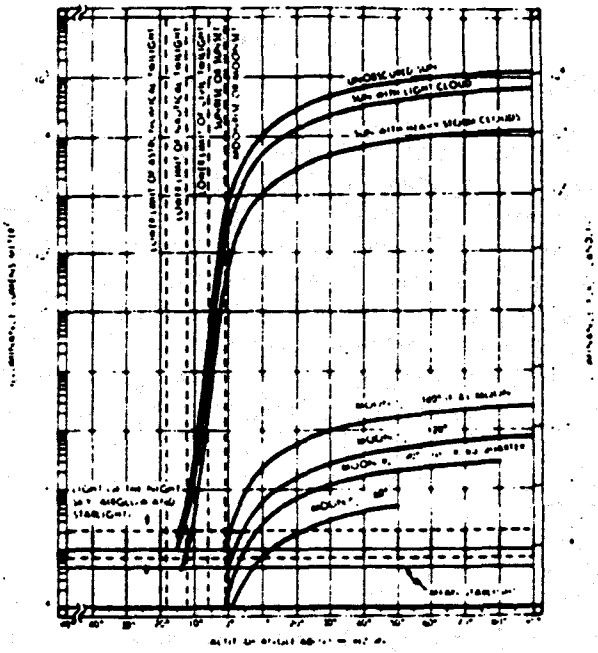

75-0440-VA-13

Figure 5. Illuminance Levels on the Surface of the Earth Due to the Sun, the Moon, and Sky[4]

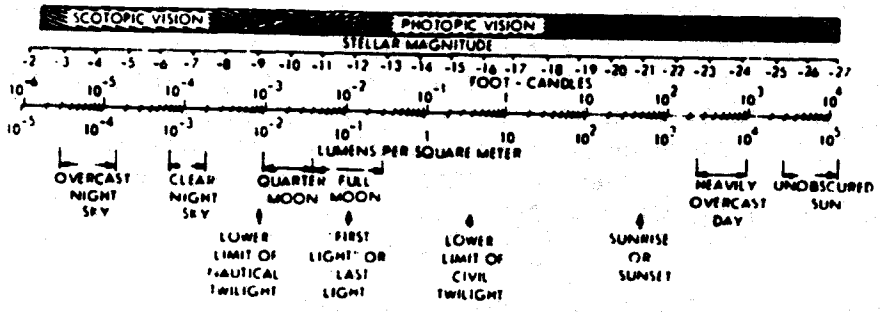


75-0440-VA-14

Figure 6. Range of Natural Illuminance Levels[4]

## 2. MODULATION TRANSFER FUNCTION (M.T.F.)

The concept of modulation transfer function (M.T.F.) has revolutionized optical system design. The M.T.F. is the system response to a sinusoidal spatial frequency input, normalized to zero spatial frequency. If we restrict the discussion to the photosensor or detector array, then the input signal is band-limited by the spacing or "pitch" of the detector elements. This follows from the Nyquist sampling theorem which states the highest spatial frequency recoverable or reconstructable in the X-direction (see figure 7) of the image has a wavelength equal to twice the pitch (i.e. $\lambda_s = 2P$). The spatial frequency, which corresponds to this limit, will be denoted as

$$\boxed{f_s(\max) = \frac{1}{2P}} \tag{16}$$

and this is the high frequency limit. In general, the output S/N of the detector array is lowest at $f_s(\max)$ and the information content in the image is often highest. We will now proceed to derive the M.T.F. for the detector array of figure 7.

If it were possible to take discrete samples of the irradiance $H(x,y)$ with perfect resolution (i.e. $\Delta X = 0$), then the Nyquist theorem states $H(x,y)$ must be sampled at least twice during each cycle of its highest spatial frequency component $f_s(\max)$. Continuing this reasoning, if the detector element amplitude resolution (i.e. detector responsivity) were infinite, then the scene would be reproduced with no loss of information up to the Nyquist spatial frequency limit given by equation (16). Since $\Delta X$ cannot be zero in practice [i.e. a finite number of photons arrive in a finite time interval and the fluctuations in their arrival sets the ultimate signal-to-noise of the detector] we will have an "error" signal generated because of spatial integration. The integrated sample at $X_0$ over the detector dimension $\Delta X$ gives the mean value of $H(X_0)$ with an error signal,

$$\Delta H(X_0) = H(X_0) - \frac{1}{\Delta X} \int_{X_0 - \Delta X/2}^{X_0 + \Delta X/2} H(X)dx \tag{17}$$

which is a measure of the uncertainty introduced for $\Delta X > 0$. Let us denote

$$H(X) = H_0 \, (1 + A \cos 2\pi f_s X) \tag{18}$$

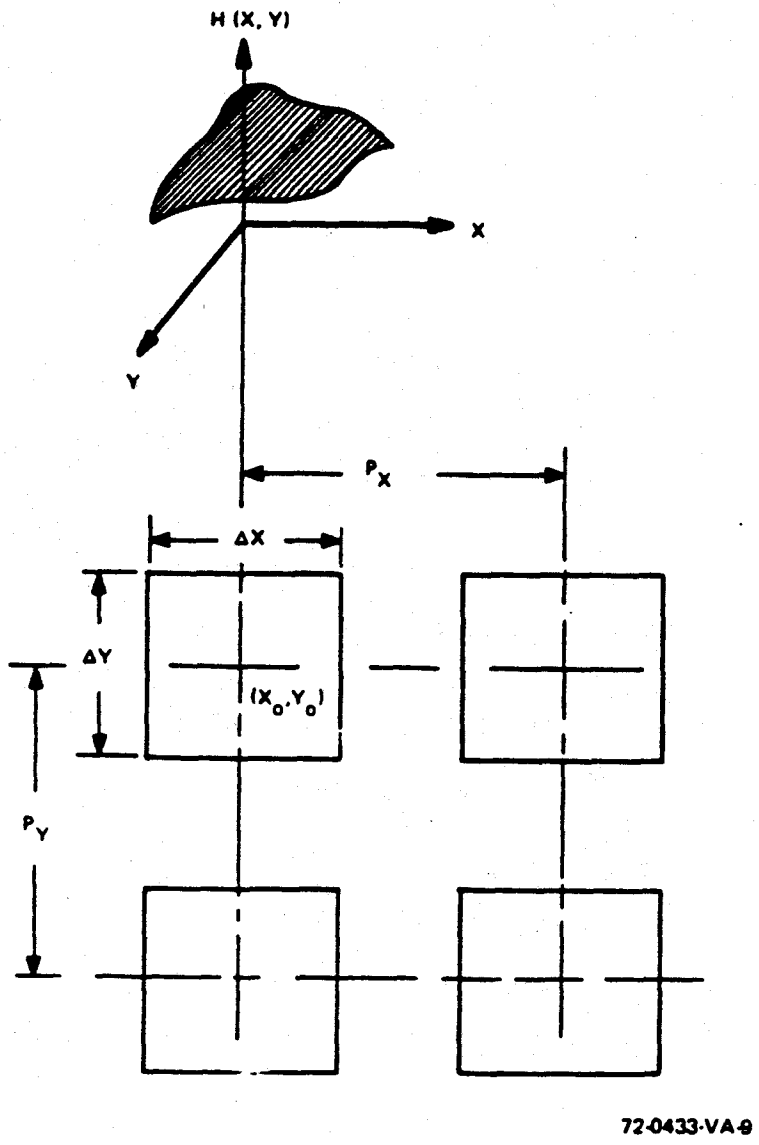


Figure 7. Irradiance on Detector Element Array

and substitution of equation (18) into (17) yields

$$\Delta H(X_o) = H_o A \left(1 - \frac{\sin \pi f_s \Delta X}{\pi f_s \Delta X}\right) \cos 2\pi f_s X_o \qquad (19)$$

$$= H(X_o) - H_m(X_o)$$

where the measured signal is

$$H_m(X_o) = H_o (1 + M \cos 2\pi f_s X_o) \qquad (20)$$

with a modulation

$$M = A \frac{\sin \pi f_s \Delta X}{\pi f_s \Delta X} \qquad (21)$$

The modulation transfer function is defined as,

$$\text{M.T.F.} \equiv \frac{M(f_s)}{M(o)} = \frac{\sin \pi f_s \Delta X}{\pi f_s \Delta X} = \frac{\sin \frac{\pi \Delta X}{2P} \quad \frac{f_s}{f_{s(max)}}}{\frac{\pi \Delta X}{2P} \quad \frac{f_s}{f_{s(max)}}} \qquad (22)$$

which is shown in figure 8 for $\Delta X = 2P$ and $\Delta X = P$.

An alternate method to derive the M.T.F. of a detector is to Fourier transform the spread function of the detector S(x).

$$S(f_s) = \int_{-\infty}^{\infty} S(x)\, e^{j2\pi f_s x} dx \qquad (23)$$

and for a spread function defined by

$$S(x) = S_o \quad \text{a constant } X_o - \frac{\Delta X}{2} \leq X \leq X_o + \frac{\Delta X}{2}$$

$$= 0 \quad \text{all other } X$$

we have

$$\text{M.T.F.} \equiv \frac{|S(f_s)|}{|S(o)|} = \frac{\sin \pi f_s \Delta X}{\pi f_s \Delta X}$$

as given in equation (22).

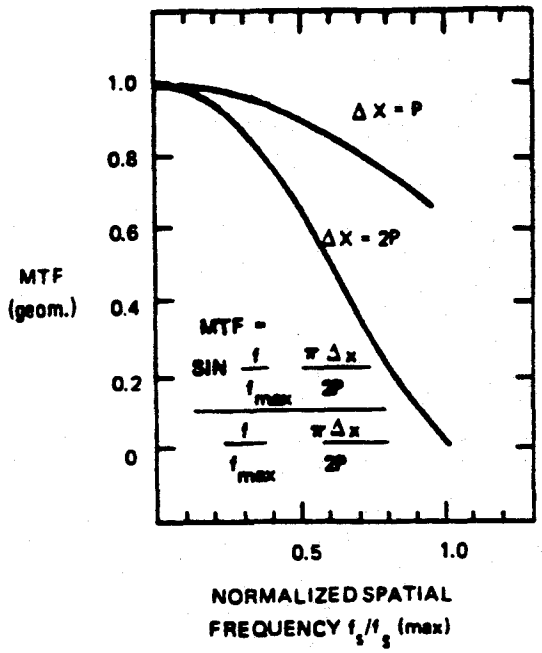


Figure 8. Modulation Transfer Function (M.T.F.) vs Normalized Spatial Frequency for $\Delta X = 2P$ and $\Delta X = P$ ($f_s(max) = 1/2P$)

## 2.1 Experimental Determination of M.T.F.

The experimental determination of M.T.F. is to slide the detector element slowly and quite accurately by means of a stepping motor past a narrow slit, which is typically demagnified to less than 5 $\mu$m including effects of lens diffraction. The detector output is amplified and drives the Y-axis of a x-y recorder while the X-axis is driven from the stepping motor. The composite profile obtained contains the slit profile as well as the sensor profile. Figure 9 illustrates the basic M.T.F. determination. To remove the slit profile from the composite profile the slit profile spread function is determined by differentiation of the edge trace produced by a knife edge scan. The Fourier transform of the slit profile spread function yields the M.T.F. of the slit image. The knife edge scan is preferred to a slit measurement since the latter suffers from low signal-to-noise ratios. The slit spread function for a 0.5 mil slit demagnified by a 1:10 lens is shown in figure 10 as a function of wavelength.

The slit image spread function $S_{Slit}(X)$ and detector spread function $S_{DET}(X)$ are slid past one another and the overlapping area produces the composite output profile given as

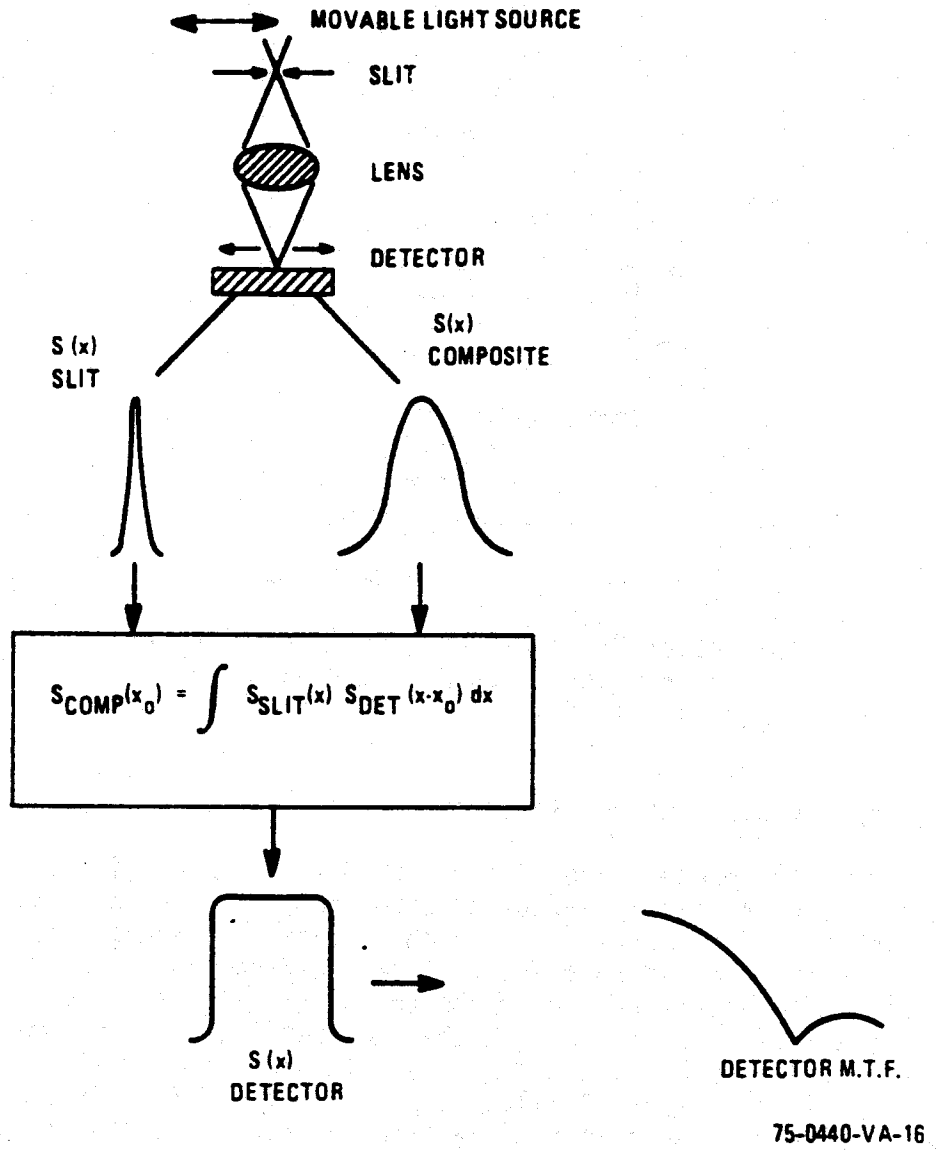


Figure 9. Modulation Transfer Function (M.T.F.) Determination

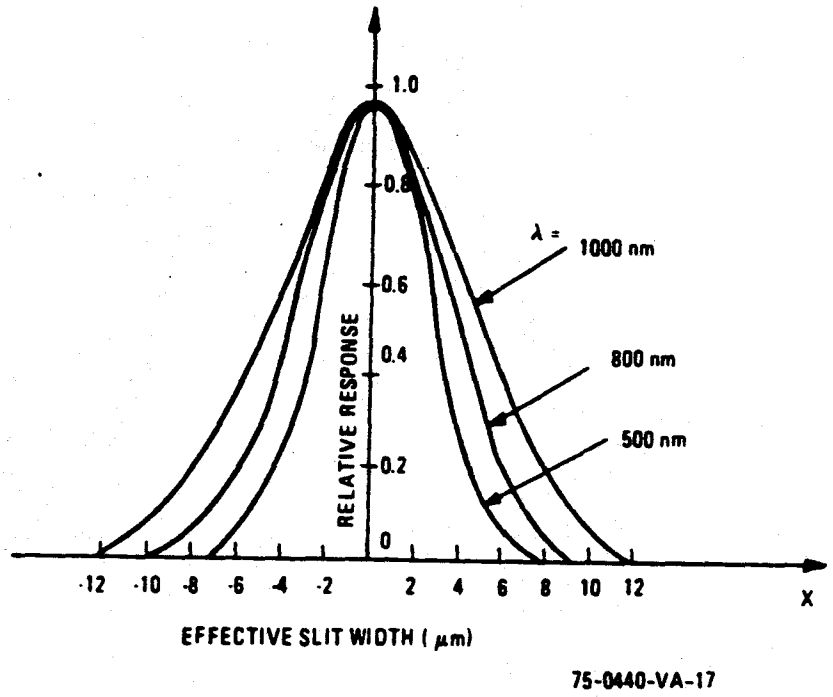


Figure 10. Slit Spread Function for a 0.5 mil Slit Demagnified by a 10X Lens Including Effects of Lens Diffraction

$$S_{COMP.}(X_o) = \int S_{Slit}(X)\, S_{DET.}(X-X_o)dx \qquad (24)$$

where $X_o$ is the coordinate of the detector center. Figure 11 illustrates the detector spread function with the effects of the slit removed through a process similar to deconvolution although equation (24) is not a convolution integral. The ideal spread function for the detector is approached at short wavelengths since the radiation does not penetrate as deep into the silicon. The effect of long wavelengths is to cause a smearing of the detector spread function and a corresponding loss in M.T.F. as illustrated in figure 12. The theoretical M.T.F. of a detector with $\Delta X = P$ at the Nyquist limit, $f_s = f_s(max)$, is given by equation (22),

$$\text{M.T.F.}\Big|_{\substack{f_s = f_s(max) \\ \Delta X = P}} = \frac{\sin \pi/2}{\pi/2} = \frac{2}{\pi} = 0.637 \qquad (25)$$

and this limit is approached as shown in figure 12.

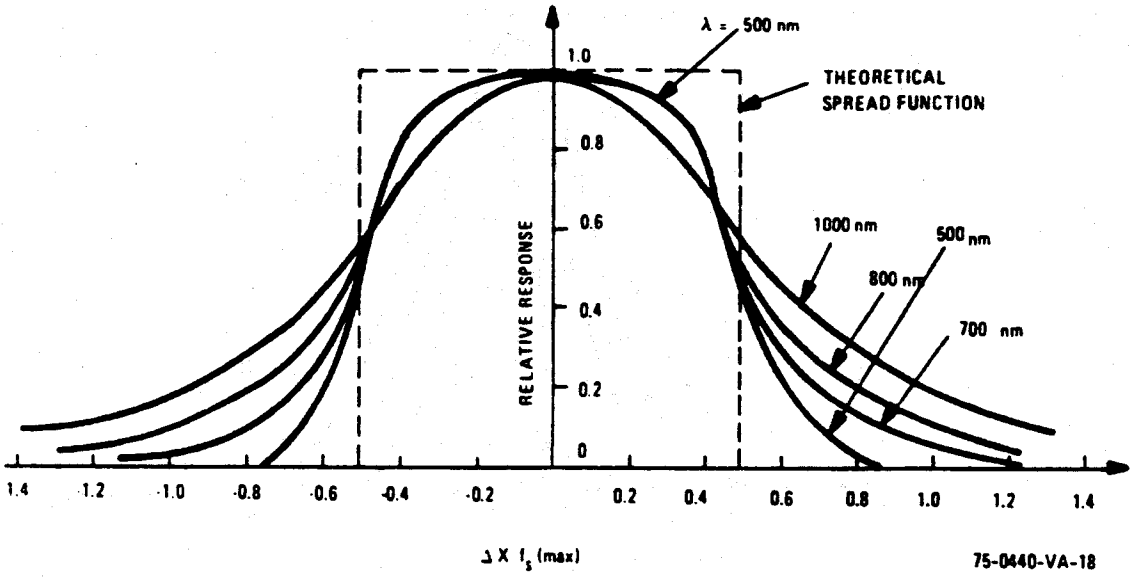


Figure 11. Detector Spread Function $S_{DET.}$ as a Function of $\Delta X f_S(max)$ and Incident Wavelength $\lambda$

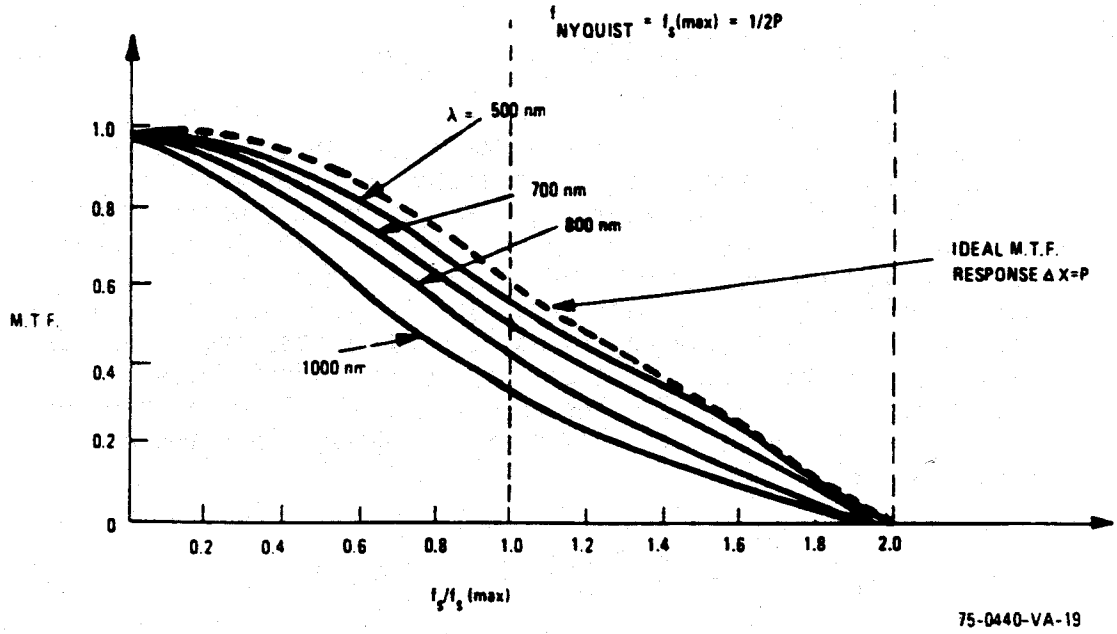


Figure 12. M.T.F. of the Detector as a Function of $f_S/f_S(max)$ and Incident Wavelength $\lambda$

## 3. NOISE CONSIDERATIONS

The low-light-level performance of a solid-state imaging system is determined by the noise equivalent signal (NES) which is the input exposure density ($\mu J/m^2$) that will provide a S/N = 1 at the system output. In order to realize the ultimate performance of the basic sensor elements (pixels), the noise introduced by the system through signal processing and conditioning must be minimized. Thus, present-day methods of signal processing use high-speed operational amplifiers followed by fast sample and hold circuits to provide signal reconstruction and automatic dark-level subtraction.[1] Figure 13 illustrates a test apparatus for the measurement of responsivity and noise. The analog signal processor consists of the input preamplifier followed by a sample and hold circuit to provide the video reconstruction shown in the output waveform. The sample and hold circuit combined with the roll-off of the amplifier filters the noise power spectrum. The measurement procedure involves a 10-bit A/D converter to sample the signal output from each pixel in the array 1,024 times at each irradiance level and record the mean and variance in A/D bits. The mean corresponds to the signal while the variance represents the noise. Linearity and streaking can be determined from the data and with narrow band optical filters the spectral response and streaking can be measured. The test apparatus of figure 13 is shown for the CCD sensor output; however, other sensor outputs interface in the same manner.

The noise is converted from A/D bits to an equivalent input exposure density ($\mu J/m^2$), called the NES, by multiplying the rms A/D bits by the reciprocal slope of the transfer curve at the particular exposure density. The reciprocal slope of the transfer curve is called the quantizing interval and is given as

$$Q_I = \frac{\Delta E}{\Delta(\text{A/D bits})} \quad \frac{\mu J}{m^2 \cdot \text{bit}} \tag{26}$$

The NES becomes

$$NES = Q_I \, B_{rms} \ (\mu J/m^2) \tag{27}$$

where $B_{rms}$ the bits variance at the specified exposure density. The NES, which is measured by this procedure, consists of four principal terms:

a. System noise from analog signal processor, power supplies, pulse jitter, mechanical vibrations, etc.

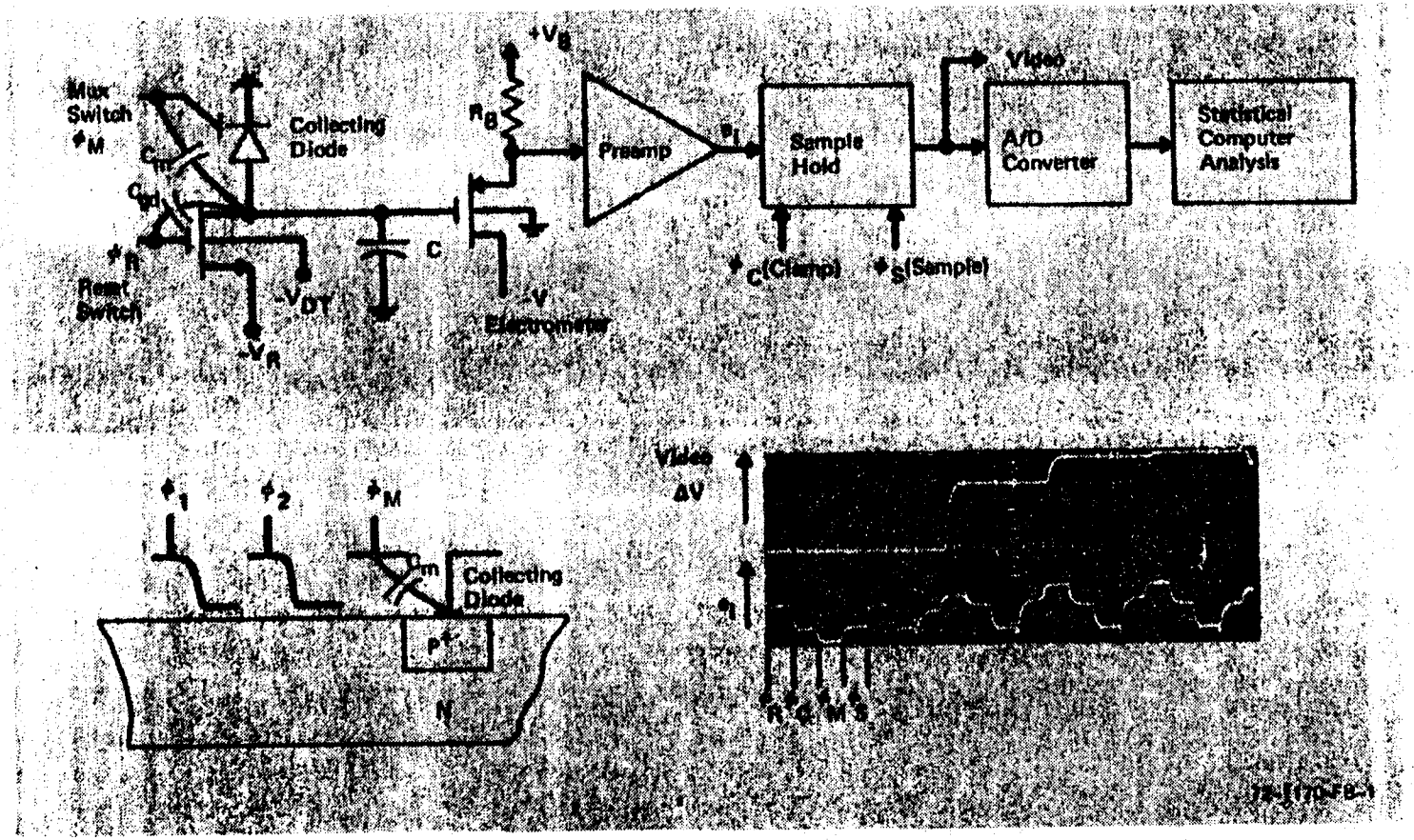


Figure 13. Measurement of Responsivity and Noise[1]

b. Chip noise from the sensor array and which is determined by the geometrical design and fabrication processes.

c. Radiation shot noise from the fluctuation in arriving signal photons.

d. Quantization noise from the uncertainty associated with the finite size of the quantizing interval $Q_I$.

The measured or total NES is given as

$$\boxed{NES^2(\text{total}) = NES^2_{\text{syst.}} + NES^2_{\text{chip}} + \frac{eE}{R_D} + \frac{Q_I^2}{12}} \qquad (28)$$

where the radiation shot noise involves the exposure density E and the quantization noise assumes an error which varies linearly with time. For a noise current $i_n$ at the input to the preamplifier in figure 13, the equivalent noise charge at the electrometer (on-chip) input is $C\, i_n/g_m$ and the noise equivalent signal associated with the system may be written as

$$NES_{\text{syst.}} = \frac{C\, i_n}{e g_m R_D} \qquad (29)$$

where $g_m$ is the transconductance of the electrometer. Thus, we note an important consideration in the reduction of system noise contributions is to increase the $g_m R_D/C$ ratio.

The $NES_{chip}$ may be formulated analytically from the following three sources of noise on the chip:

a. Nyquist noise of reset and address switches with noise charge $Q_n^2 = kTC$, where C is a node capacitance or "well" capacitance for input CCD noise.

b. Shot noise associated with sensor, switches, or shift register (for CCD's) thermal leakage currents with noise charge $Q_n^2 = eI_L\tau$, where $\tau$ is the exposure time and $I_L$ the leakage current.

c. Surface trap and bulk trap noise associated with the sensor, output electrometer, or shift register (for CCD's) and which may be written as $Q_n^2 = kTC_t$ where $C_t$ is an effective trap capacitance.

With these terms the chip NES becomes

$$NES_{chip} = \frac{\left[kT\ (C + C_t) + eI_L\tau\right]^{1/2}}{R_D} \qquad (30)$$

The above expression is modified to include an $R(1-\epsilon)^N$ for CCD's due to the finite transfer inefficiency $\epsilon$ and the number of transfers N. A principle limitation to the $NES_{chip}$ is the Nyquist noise of the output reset switch, which gives an rms pixel noise charge of 200 $e^-$ for a 0.25 pF output capacitance. This limitation has been removed in CCD imagers with a method of signal processing called correlated double sampling[1] in which two samples are taken within a pixel time window. This method can be used to approach the limiting case of shot-noise for buried-channel CCD imagers; however, the surface channel CCD imagers are limited by the need to inject an electrical fat zero which gives a kTC contribution at the input injection circuit.

## 3.1 Correlated Double Sampling[1]

A method of signal processing called correlated double sampling has been developed which removes the switching transients at the output collection diode of a CCD, eliminates the Nyquist noise of the reset switch-output capacitance combination, provides dc restoration and increases dynamic range, and suppresses surface state and 1/f noise contributions.

Let us examine the four distinct timing intervals employed in the readout circuit of figure 14.

1. Reset

The n-channel MOSFET reset switch is turned on the voltage $V_G$ across the capacitor C is reset to the reference voltage $V_R$ with a noise uncertainty $V_n$. This noise voltage may be introduced through inadequate filtering of the reference supply voltage and the Nyquist noise contribution of the reset switch, [9], [10] where the latter is given by $V_n = (kT/C)^{1/2}$ or in terms of noise charge $Q_n = (kTC)^{1/2}$. The full Nyquist voltage appears across C when the electrical time constant formed by the series resistance of the reset switch and integration capacitance C is much less than the time the reset switch is on. The p-channel electrometer is connected to an operational amplifier which is the preamplifier in the CCD signal processor circuit shown in figure 15. The timing diagram for the signal processing is illustrated in figure 16. At the start of the reset interval the pixel charge is in transit to the last well (i.e., see phase $\phi_2$ and figure 14) of the electrical bit adjacent to the mux gate $\phi_M$ and the collection diode.

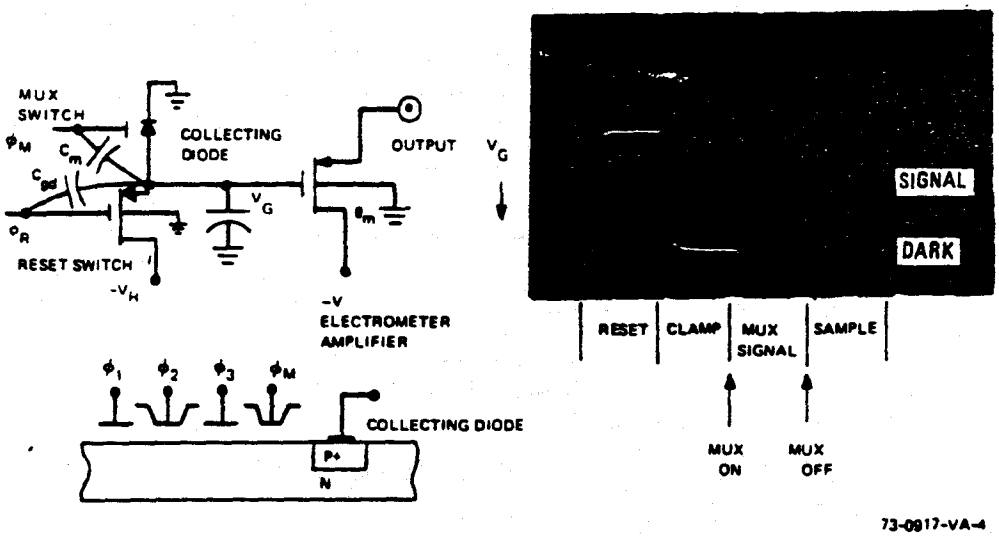


Figure 14. CMOS Correlated Double Sampling Readout Circuit[1]

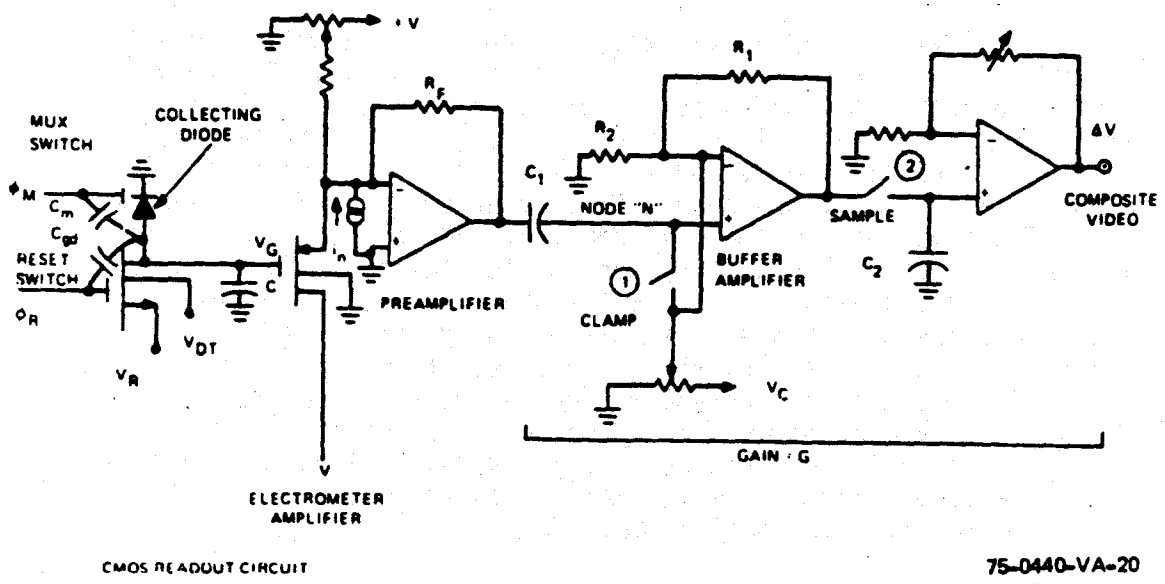


Figure 15. Schematic Diagram of a CDS Processor with Critical Capacitances, Noise Sources, and Signal Nodes[1]

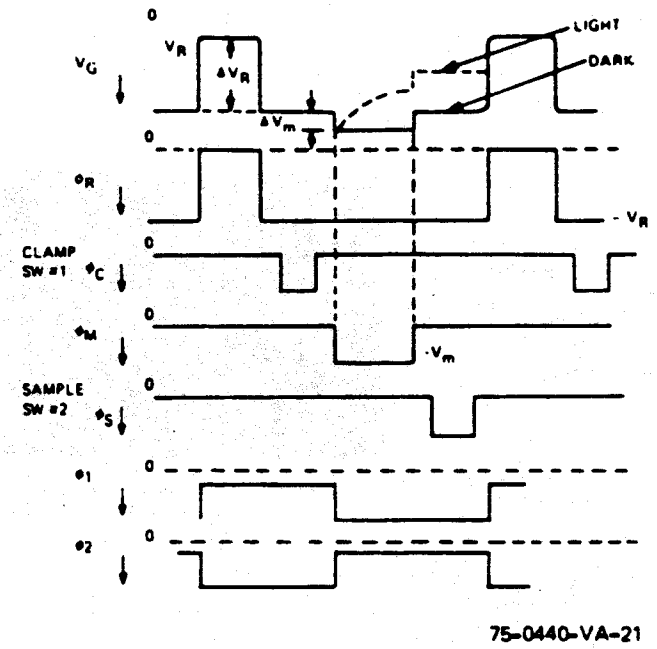


Figure 16. Timing Diagram for CCD Line Array with CDS Analog Signal Processor. The Four Steps are Separated in Sequence to Correspond to Explanation in the Text[1]

2. Read Reset

After the n-channel reset switch is turned off, the voltage present on the gate of the electrometer consists of a feedthrough pedestal $\Delta V_R$ and a noise voltage $V_n$. With the reset switch off, the gate voltage is holding on a high impedance point with a time constant of seconds. In the read reset interval, the clamp switch 1 is turned on and $C_1$ is charged to a voltage indicative of the voltage on the electrometer. Switch 1 is turned off and one side of the capacitor, node N, is clamped or dc restored to a reference voltage $V_c$, while the other side of the capacitor represents the instantaneous sample of the gate voltage. The instantaneous voltage across the clamp switch from this moment on is the differential or incremental charge caused by a change in the on-chip gate or collection diode voltage. With the clamp switch turned off, the measured reset level is holding on the high impedance node N formed by the clamp capacitor $C_1$, and the noninverting input of the buffer amplifier.

3. Mux Signal

At the start of the mux signal interval the pixel charge is raised in the storage well ($\phi_2$ goes high) and $\phi_M$ goes low to

transfer the pixel charge to the collection diode. The collection of pixel charge (minority carriers) discharges the voltage $V_G$ as shown in the signal waveform of figure 14. If we assume, for the moment, there is no pixel charge, then the only charge transferred to the gate electrode is the feedthrough pedestal $\Delta V_m = V_m C_m/C$, where $V_m$ is the mux voltage swing and $C_m$ the feedthrough capacitance from the mux gate to the collection diode. The charge is removed, however, when the mux gate is turned off as shown in figure 14. A Nyquist noise of $Q_n^2 = 2kTC_m$ is introduced, which may be minimized for $C_m < 0.01$ pF for the case where the mux gate does not overlap the collection diode. Alternatively, an overlapping mux gate $\phi_m$ may be held at a fixed dc potential with the clock $\phi_2$ transferring charge to the collection diode (see figure 14). In the absence of any optical pixel charge we would collect the leakage current from the sensor and the shift register wells.

4. Read Signal

After the mux signal is turned off, the running output voltage on node N is the time difference between the previously clamped reset level and the same reset level plus signal increment introduced by the closure of the mux switch (i.e., there is negligible leakage of the reset level between read reset (clamp) and read signal (sample) intervals). Thus, the reset noise, which includes Nyquist noise and $V_R$ power supply noise, is correlated within a pixel time window. The signal increment, which consists of sensor and shift register leakage current added to photocharge, is amplified and passed to the output of the signal processor by the closure of the sample switch 2. The output video stream is a sequence of pixel element responses free from reset noise and proportional to the minority carrier signal increment introduced by closure of the mux switch.

The correlated double sampling (CDS) method removes switching transients similar to an earlier technique [5] which used a gated charge integrator in lieu of storing (clamping) the actual diode reset level for subsequent subtraction from the reset level plus signal increment to give the signal increment without reset noise. The Nyquist noise of the reset switch has been removed since it is correlated within a pixel time, and this means a removal of a noise charge

$$Q_n = \frac{(kTC)^{1/2}}{e} = 200e^-$$

for a 0.25 pF capacitor. The "1/f" surface-state noise is also suppressed by the filter characteristic of the analog signal processor which is shown as follows.

The transfer function, which acts on any time-varying components of the signal between clamp and sample intervals, may be written as

$$T(s) = T_0 \frac{(1 - e^{-s\tau})}{1 + s/\omega_0} \tag{31}$$

where $T_0$ is the signal gain and $\tau$ is the delay time between the end of the clamp pulse and the end of the sample pulse, and $\omega_0$ is the bandwidth of the front-end preamplifier. Figure 17 illustrates a plot of the filter characteristic for a value of $\tau = T/2$, where T is the clock period. The important features of this filter are the "double zeros" of $|T(\omega)^2|$ at $\omega = 2N\pi/T$ (N = 0,1,2,...). The "double zero" at the origin ($\omega = 0$) serves to suppress 1/f and and low frequency noise arising from power supplies, pulse jitter, etc, and the double zero at even harmonics of the fundamental clock frequency also suppresses surface-state noise generation in the p-channel MOS electrometer amplifier. Thus, the signal processing does not degrade but enhances the qualities of the sensor element by removing the Nyquist noise and filtering the 1/f noise while amplifying the signal. In addition to these features, we have automatic dark level subtraction to increase the dynamic range since the video signal is clamped by the reference voltage $V_c$. There is no need to filter out the clock fundamental and higher order harmonics; and the video output is already in a format for image display or further data processing.

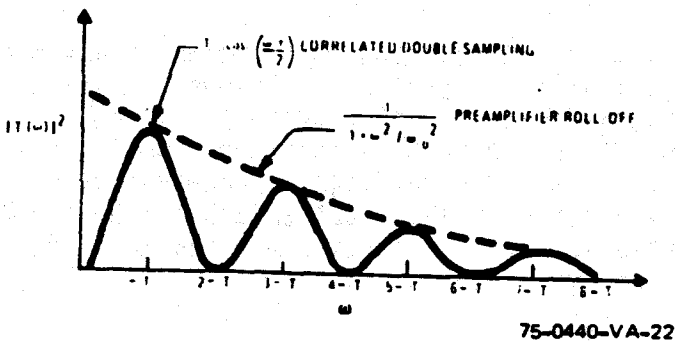


Figure 17. Filter Characteristics of CDS Analog Processor with $\tau = T/2$

## 4. FIGURE OF MERIT F.M. = S/N x M.T.F. (eff.)

In the design of low light level image arrays we must concentrate on two important quantities: (1) sensitivity and (2) resolution. The sensitivity can be described by the noise equivalent signal (NES) discussed in section 3 and represented by the signal-to-noise ratio given by equation (28). The resolution is described in terms of the observable spatial resolution (line pairs/mm or lines/mm) at a certain contrast level or system gain. This design parameter is called the modulation transfer function or M.T.F. and the use of it has revolutionalized optical system design. The M.T.F. is the modulus of the optical transfer function which is the system response to a sinusoidal spatial frequency input $f_s$ band-limited by the sensor element spacing or pitch P. Let us examine the sensor line array shown in figure 7 with $\Delta Y$ in the along-track direction and $\Delta X$ in the across-track direction. The image or scene moves in the along-track direction while the line array is scanned electronically in the across-track direction. The modulation transfer function in the across-track direction is from equation (22)

$$M.T.F._x = \frac{\sin(\pi f_s \Delta X)}{\pi f_s \Delta X} \tag{32}$$

and in the along-track direction

$$M.T.F._y = \frac{\sin(\pi f_s \nu\tau)}{\pi f_s \nu\tau} \cdot \frac{\sin(\pi f_s \Delta Y)}{\pi f_s \Delta Y} \tag{33}$$

where $\nu$ is the velocity of the scene across the image plane and $\tau$ the exposure (line) time (i.e., $d = \nu\tau$ is the distance the image moves during the exposure time). The additional term in equation (33) is due to the relative motion between the image and sensor during the time the output signal is generated.

If the noise is determined by the first signal preamplifier, then to a first-order approximation the noise is independent of detector area and the S/N ratio increases proportional to the detector area,

$$S/N \sim \Delta X \, \Delta Y \tag{34}$$

If we make the assumption the effective resolution (M.T.F.) is the geometric mean of its components, then a figure-of-merit may be defined as[6]

$$\text{figure-of-merit (F.M.)} \equiv \Delta X \Delta Y \left[ (\text{M.T.F.}_x)\ (\text{M.T.F.}_y) \right]^{1/2} \sim \text{S/N M.T.F. (eff.)} \quad (35)$$

The F.M. may be maximized at the Nyquist limit $f_s(\max) = 1/2P$ and letting $\nu\tau = P$ to conserve bandwidth and provide two samples in the along-track direction. With these conditions the F.M. becomes,

$$\text{F.M.}\Big|_{f_s=f_s(\max)} = \Delta X \Delta Y \left[ \frac{\sin\left(\frac{\pi \Delta X}{2P}\right)}{\left(\frac{\pi \Delta X}{2P}\right)} \right]^{\frac{1}{2}} \left[ \frac{2}{\pi} \frac{\sin\left(\frac{\pi \Delta Y}{2P}\right)}{\left(\frac{\pi \Delta Y}{2P}\right)} \right]^{\frac{1}{2}} \quad (36)$$

Differentiation of equation (36) with respect to $\Delta Y$ yields

$$\tan \frac{\pi \Delta Y}{2P} = - \frac{\pi \Delta Y}{2P} \quad (37)$$

with a solution

$$\Delta Y = 1.292P \quad (38)$$

as the optimum value for the along-track dimension. Equation (36) is plotted in figure 18 with the value $\Delta X/P$ varied and $\Delta Y = 1.292P$ held constant at its optimum value. To the left of the peak the detector has a high M.T.F. but a low S/N with the converse true to the right of the peak. For $\Delta X/P > 1$ a bilinear array is required, rather than a true linear array, with an offset in the along-track direction as shown in the 2-P offset of figure 19. The offset must be an integer multiple of P in order to reconstruct the image on a uniform Cartesian grid. In situations where aliasing is expected to present a problem the bilinear array offers optimum performance since at $\Delta X = 2P$ there is no response and aliasing effects are minimized. Another consideration in the selection of a bilinear, maximum-performance array is the need to avoid excessive image misregistration in either the x or y components due to angular deviations from perpendicularity to the array of the image velocity vector. This would necessitate small spacings between the two rows of detectors.

## 4.1 Equiresolution Bilinear Array

In applications, such as cartography, equal resolution is required in both the across-track and along-track directions. Thus, we can set the M.T.F.'s equal at the limiting spatial frequency $f_s(\max)$ and let $\nu\tau = P$ to conserve bandwidth to find,

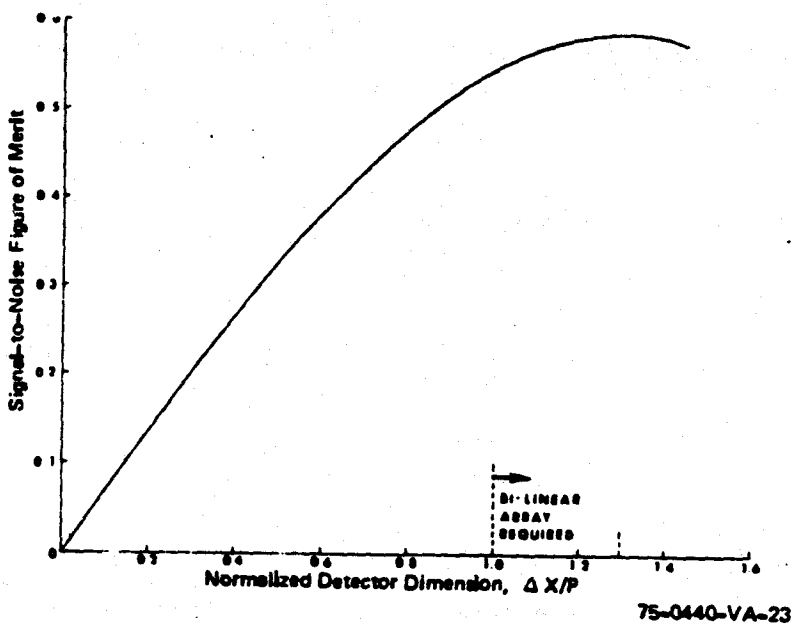


Figure 18. Figure-of-Merit[6] as a Function of ΔX/P

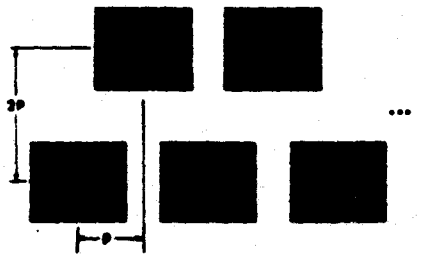


Figure 19. Bilinear Detector Element Array for Maximum Performance

$$\frac{\sin\left(\frac{\pi\Delta X}{2P}\right)}{\left(\frac{\pi\Delta X}{2P}\right)} = \frac{2}{\pi}\,\frac{\sin\left(\frac{\pi\Delta Y}{2P}\right)}{\left(\frac{\pi\Delta Y}{2P}\right)} \tag{39}$$

Equation (39) provides the relationship between $\Delta X/P$ and $\Delta Y/P$ to obtain equal resolution in both x and y directions. Thus, the F.M. becomes

$$\text{F.M.}\Big|_{f_s(\max)} = \frac{4\Delta X P}{\pi^2}\sin\left(\frac{\pi\Delta Y}{2P}\right) \tag{40}$$

subject to the constraint of equation (39). The equiresolution bilinear array has a maximum F.M. with the values

$$\begin{aligned} \Delta X &= 1.45P \quad \text{(preamplifier noise-limited)} \\ \Delta Y &= 1.17P \end{aligned} \tag{41}$$

as shown in figure 20. The M.T.F. of $f_s(\max)$ is 0.33 for the conditions above and if we desire P = 15 $\mu$m, then $\Delta X$ = 22 $\mu$m and $\Delta Y$ = 18 $\mu$m are logical selections to achieve a maximum performance

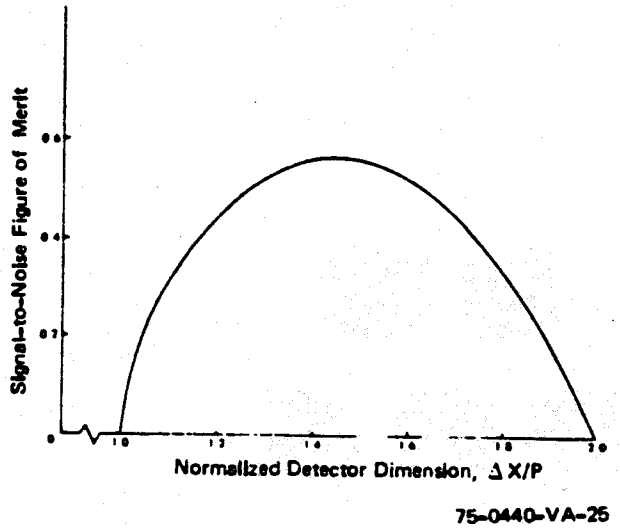


Figure 20. Figure-of-Merit of Equal Resolution Bilinear Array[6]

linear detector array. The M.T.F. deviation between along and cross track is minimal as shown in figure 21. Figure 22 illustrates a 2P bilinear CCD array (P = 15 $\mu$m) with the design indicated by equation (41) and defined by an aluminum light shield.

If the detector array has very low noise and the detector area limits the noise through such factors as thermal "shot" noise $(eI_L\tau)^{1/2}$, Nyquist noise $(kTC_D)^{1/2}$ or radiation "shot" noise $\left(\frac{eE}{R_D}\right)^{1/2}$, then the signal-to-noise ratio becomes

$$S/N \sim (\Delta X \Delta Y)^{1/2} \tag{42}$$

and the optimum set of values are

$$\begin{aligned} \Delta X &= 1.26P \qquad \text{(detector area noise-limited)} \\ \Delta Y &= 0.85P \end{aligned} \tag{43}$$

which yields a M.T.F. = 0.46 at $f_s$(max). For P = 15 $\mu$m the dimensions of the low-noise bilinear array are $\Delta X$ = 19 $\mu$m and $\Delta Y$ = 13 $\mu$m. Such an array could be designed with a 1-P offset in the along-track direction to minimize misregistration of the image as discussed previously. In this design the aliasing will be decreased since the spatial sampling frequency is higher in the along-track direction.

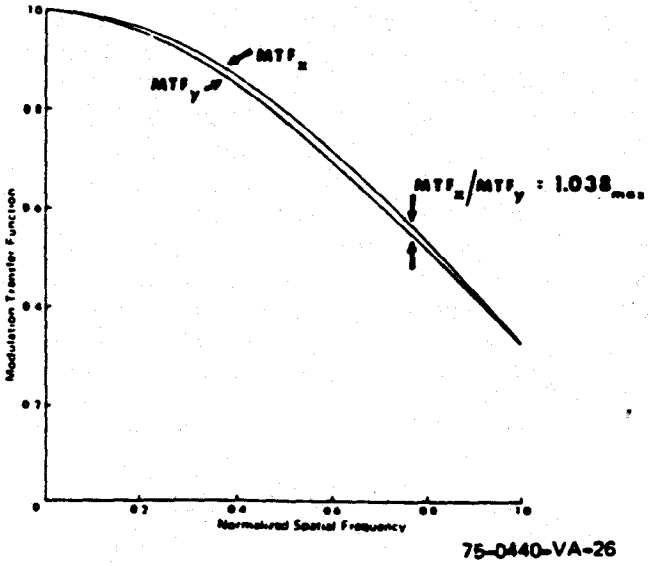


Figure 21. Illustration of Similarity of x and y Modulation Transfer Functions for Bilinear Equiresolution Array[6]

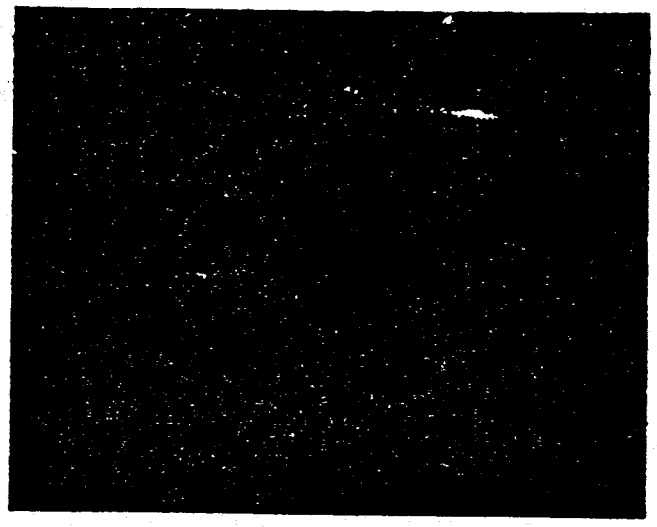

Figure 22. 2P - Bilinear Offset CCD Array P = 15 $\mu$m; $\Delta X$ = 22 $\mu$m; $\Delta Y$ = 18 $\mu$m

## 4.2 Maximum Performance Linear Array

We have discussed the bilinear detector array with 1-P and 2-P offsets in the along-track direction for bandwidth conserving $\nu\tau = P$. In this section we will examine the zero offset case (i.e., 0-P) which corresponds to a linear array of elements, Since $\Delta X = P$ the $M.T.F._x$ is constrained and we need an adjustable parameter to obtain equiresolution at the Nyquist limit $f_s(max)$. An examination of equations (32) and (33) indicates for $\nu\tau = P$ we must have $\Delta Y \longrightarrow 0$ for equiresolution. Alternately, if we select $\Delta Y = P$, then $\nu\tau \longrightarrow 0$ is required for equiresolution. In the first case there will be appreciable signal reduction and in the second case the bandwidth requirements are considerable. If we simply constrain $\nu\tau = P$ and formulate the figure-of-merit F.M., then from equations (32), (33) and (35) we have,

$$F.M.\Big|_{f_s(max)} = P^2 \left(\frac{2}{\pi}\right)^{3/2} \left[\left(\frac{\Delta Y}{P}\right) \sin\left(\frac{\pi \Delta Y}{2P}\right)\right]^{\frac{1}{2}} \qquad (44)$$

for the preamplifier noise-limited case. The maximum F.M. occurs with the selection

$$\begin{aligned} \Delta X &= P \qquad \text{(preamplifier noise-limited)} \\ \Delta Y &= 1.292P \end{aligned} \tag{45}$$

with a $M.T.F._x = 2/\pi$ (0.637) and $M.T.F._y = 0.28$. For the case of detector noise-limited performance the F.M. becomes,

$$F.M.\Big|_{f_s(max)} = P\left(\frac{2}{\pi}\right)^{3/2} \sin^{\frac{1}{2}}\left(\frac{\pi\Delta Y}{2P}\right) \tag{46}$$

with maximum value at

$$\Delta X = \Delta Y = P \qquad \text{(detector noise-limited)} \tag{47}$$

and a $M.T.F._y = 0.41$. Thus, for $\Delta X = P = 15\ \mu m$ the value of $\Delta Y$ may range from 15 $\mu$m to 20 $\mu$m, the exact value determined by the partitioning of noise between the detector and the preamplifier. Figure 23 illustrates a 0-P photodiode array with $\Delta X = P = 15\ \mu m$ and $\Delta Y = 20\ \mu m$.

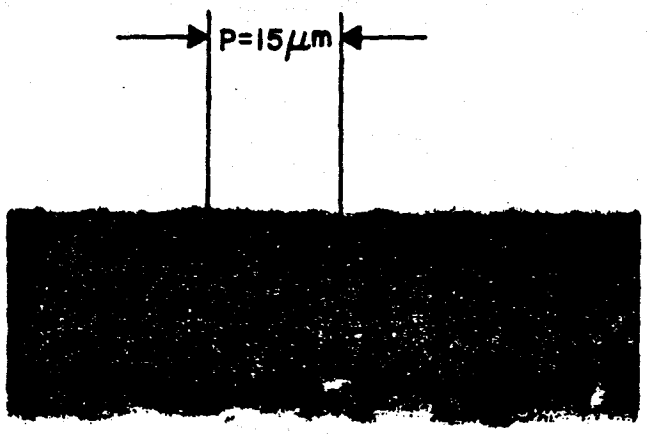


Figure 23. Linear Photodiode Array $\Delta X = P = 15\ \mu m$; $\Delta Y = 20\ \mu m$;

## 4.3 Other M.T.F. Considerations

In general, there are three M.T.F. factors in sensor design:

- geometrical M.T.F.
- diffusion M.T.F.
- transfer inefficiency M.T.F.

We have discussed the geometrical M.T.F. associated with the aperture definition of the sensor. The diffusion M.T.F. is a result of the penetration of the incident radiation into the silicon with subsequent diffusion of the charge carriers from the point of generation to the depletion region of the reverse-biased diode.

Figure 24 illustrates a cross section of a photodiode sensor array with pitch P. The long wavelength radiation penetration into the silicon is described by the incident flux density at a given wavelength $\lambda$ as

$$N_\lambda = \frac{N_0(\lambda)}{2}\left(1 + \cos 2\pi f_s x\right)\left(1-r(\lambda)\right)e^{-\alpha(\lambda)y} \qquad (48)$$

where $N_0$ is the peak photo flux, $r(\lambda)$ the reflection coefficient of the silicon and $\alpha(\lambda)$ the absorption coefficient as shown in figure 25. The spatial variation with x as indicated in equation (48) is for the calculation of the M.T.F. The diffusion equation, which describes the movement of photogenerated carriers may be written as,

$$-D\nabla^2 p + p/\tau = G(x,y) = \frac{\partial N_\lambda}{\partial y} \qquad (49)$$

where $p(x,y)$ is the excess minority carrier density, D the diffusion coefficient, and $\tau$ the bulk recombination lifetime. The current density for the photodiode may be written in the form[7]

$$J_\lambda = \frac{eN_0(\lambda)}{2}\left[n(o) + n(f_s)\cos 2\pi f_s x\right] \qquad (50)$$

where $n(o) = n(f_s = o)$ and the M.T.F. is,

$$\text{M.T.F. (diffusion)} = \frac{n(f_s)}{n(o)} \qquad (51)$$

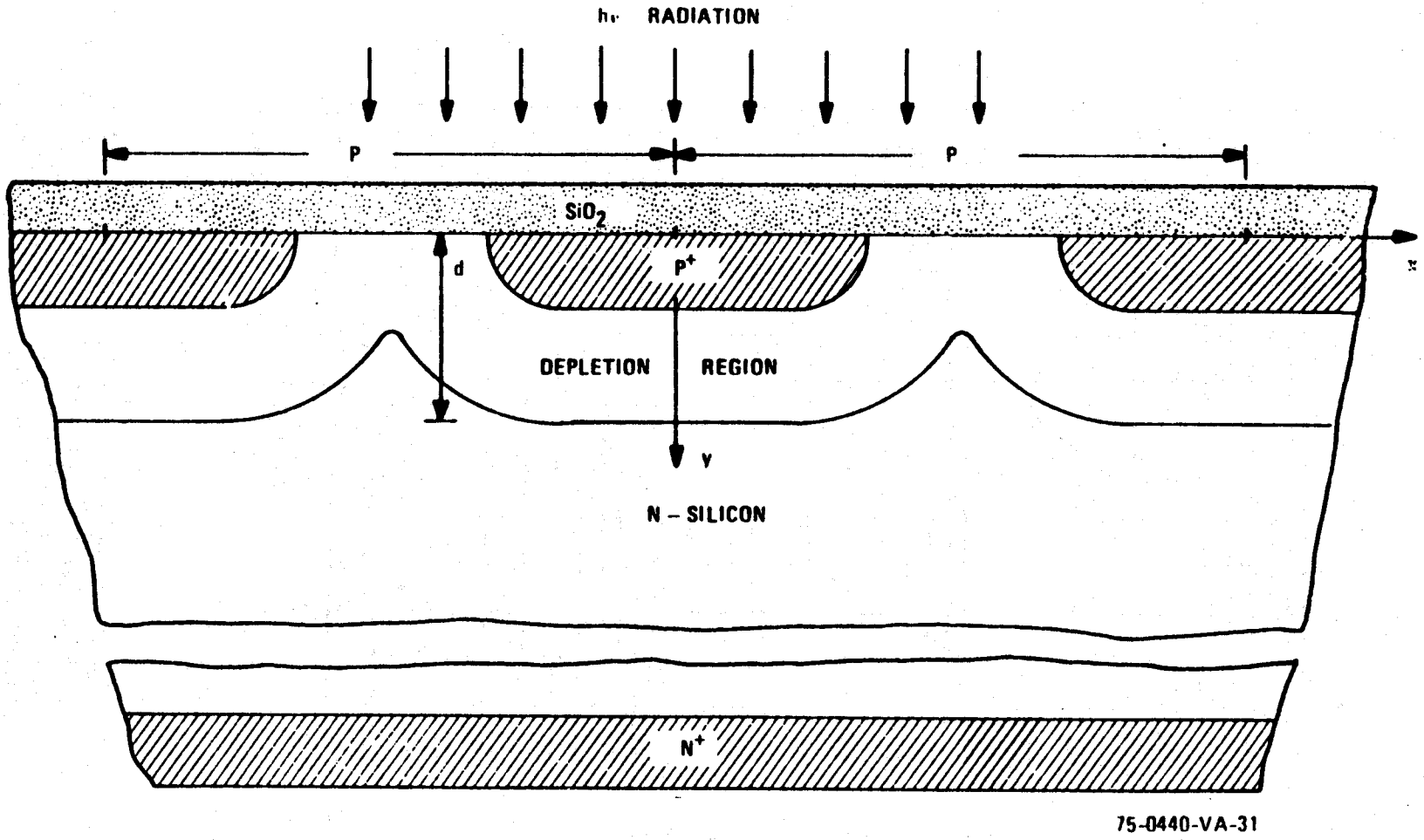


Figure 24. Cross Section of a Photodiode Sensor Array with Pitch P

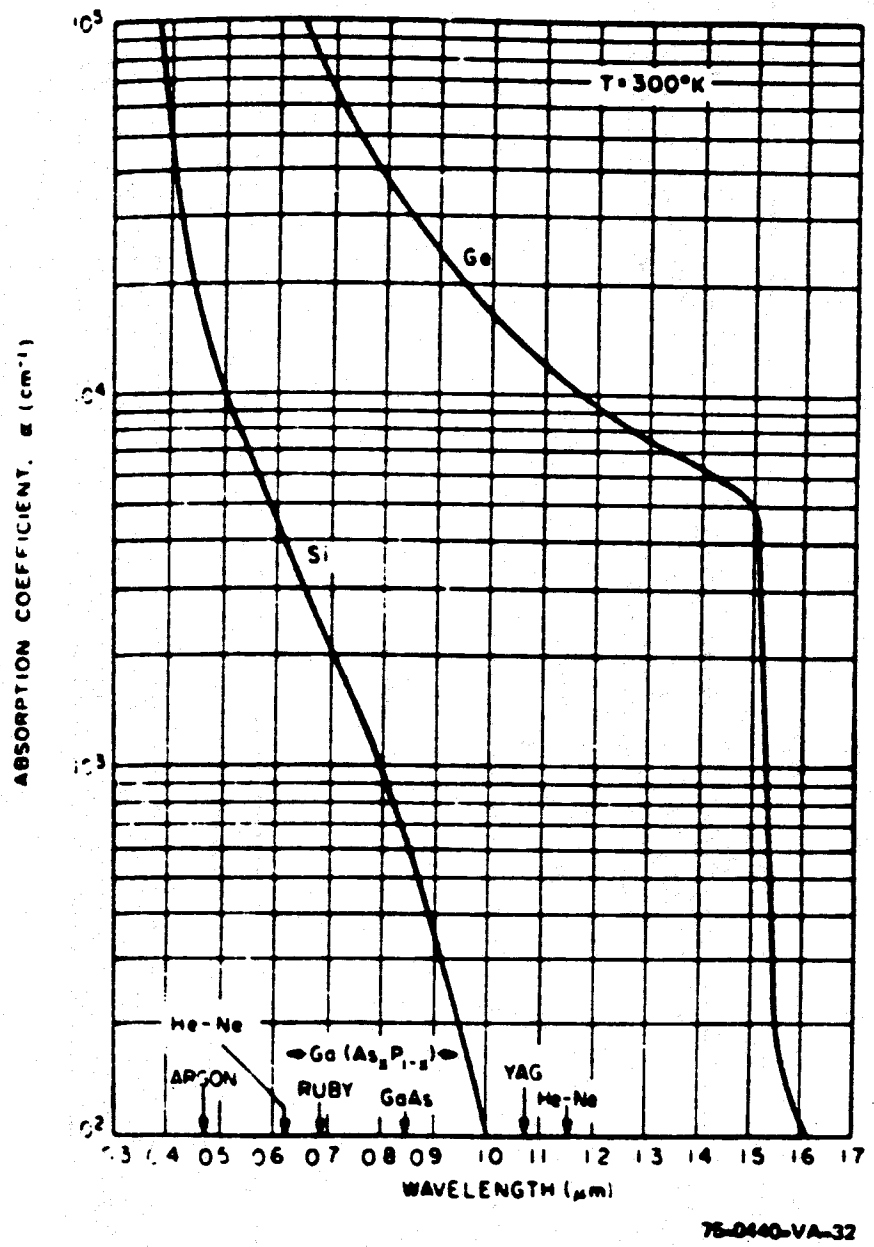


Figure 25. Absorption Coefficient vs Wavelength for Ge and Si at 300°K [After W.C. Dash and R. Newman, "Intrinsic Optical Absorption in Single Crystal Germanium and Silicon at 77°K and 300°K," Phys. Rev., 99, 1151, (1955)]

If we assume the junction depth d is thin, such that negligible trapping of photogenerated charge carriers occurs in the $P^+$ region, then we may solve the boundary value problem of a depletion region with

$$P = 0 \quad \text{at } y = d \text{ and } y = \infty \tag{52}$$

The hole flux entering the $P^+$ region $J_\lambda(x)$ may be calculated by evaluating the hole diffusion current density that enters the depletion region and adding to this quantity the photogenerated holes absorbed in the depletion region width d. Essentially we assume all the photogenerated carriers within the depletion region are collected efficiently and no excess carrier buildup is possible since the high electric field sweeps the carriers out of this region. Thus, we need only concern ourselves with the photogenerated carriers outside the depletion region and their wavelength and spatial frequency dependence. The value of M.T.F. becomes,

$$\text{M.T.F (diffusion)} = \frac{1 - \frac{e^{-\alpha d}}{1+\alpha L}}{1 - \frac{e^{-\alpha d}}{1+\alpha L_o}} \tag{53}$$

where $\frac{1}{L^2} = \frac{1}{L_o^2} + (2\pi f_s)^2$ and $L_o^2 = D\tau$. Typical values for a photodiode sensor array are d = 5 $\mu$m, $L_o$ = 50 $\mu$m and P = 15 $\mu$m, where $f_s(\max) = 1/2P$. Figure 12 illustrates the influence of $\alpha(\lambda)$ on the M.T.F.

The CCD sensors have a M.T.F. degradation due to the finite transfer inefficiency $\epsilon$ associated with each transfer. The transferred charge is added to trailing samples which causes a dispersive effect on the output signal. We can derive the M.T.F. due to tranfer inefficiency through the discrete recursive relation[8] for the signal charge in a delay line

$$q_s(X,t) = \epsilon\, q_s(X,t-1) + (1-\epsilon)\, q_s(X-1,t-1) \tag{54}$$

where X and t are normalized to the CCD cell pitch P and clock time $T_c$, respectively. Since equation (54) is a discrete set of signal values in the time domain, we can transform the signal to the Z-domain.

$$Q_s(X,Z) = Z^{-1}\left[\epsilon Q_s(X,Z) + (1-\epsilon)\, Q_s(X-1,Z)\right] \tag{55}$$

where $Z = e^{ST_c}$ and S is the complex frequency. We can calculate the transfer function after N transfers as,

$$\left[\frac{Q_S(X,Z)}{Q_S(X-1,Z)}\right]^N = \left[\frac{(1-\epsilon)Z^{-1}}{1-\epsilon Z^{-1}}\right]^N \simeq e^{-N\epsilon(1-Z^{-1})} \tag{56}$$

and the M.T.F. is determined with the substitution $Z = e^{j2\pi f_S/f_c}$ where $f_c = 2f_S(\max)$. The M.T.F. becomes

$$\text{M.T.F. (transfer inefficiency)} \doteq e^{-N\epsilon\left[1-\cos \pi f_S/f_S(\max)\right]} \tag{57}$$

which is illustrated in figure 26.

The actual M.T.F. used in the design approach must be the composite of all three M.T.F.'s discussed in this section. Thus, for a CCD imager we must write the M.T.F. as,

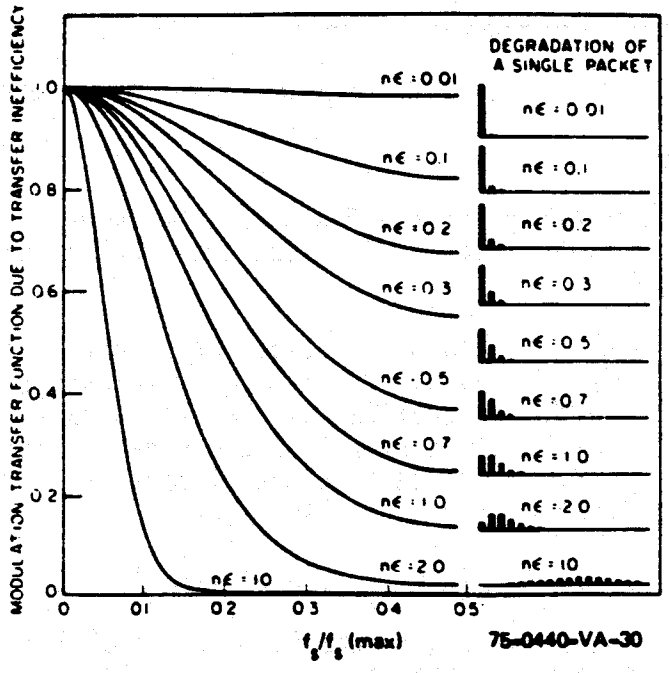


Figure 26. Degradation in M.T.F. Due to Various Values of Nε as a Function of Normalized Frequency[10]

$$M.T.F._x = e^{-N\epsilon\left[1-\cos \pi f_s/f_s(max)\right]} \cdot \frac{1 - \frac{e^{-\alpha d}}{1+\alpha L}}{1 - \frac{e^{-\alpha d}}{1+\alpha L_o}} \cdot \frac{\sin \frac{\pi f_s \Delta x}{2Pf_s(max)}}{\frac{\pi f_s \Delta x}{2Pf_s(max)}} \quad (58)$$

instead of the single geometrical M.T.F.

## 4.4 Area Array Design

The design of an area array proceeds along the same direction as discussed previously for the line array. The F.M. is formed for the sensor,

$$F.M. = \Delta X \Delta Y \left(M.T.F._x \, M.T.F._y\right)^{1/2}$$

where the $S/N \sim \Delta X \Delta Y$ and preamplifier noise-limited performance is assumed. The area will not have the relative image velocity correction term since the array is electronically scanned in both x and y directions. In TV applications the format of the array is limited to a 4:3 aspect ratio to reconstruct the image for the observer. Furthermore, the video bandwidth restrictions combined with the need to provide a "flicker-free" picture for human viewing (i.e., 30 frames/sec interlaced 2:1), determine the number of picture elements (pixels) in the array. Further restrictions are placed by horizontal and vertical "retrace" intervals which limit the number of usable TV lines/raster height and horizontal resolution.

# 5. STREAKING CONSIDERATIONS

Streaking in the image may be caused by the following:

- temperature - nonuniform increase in leakage current with temperature fluctuations
- responsivity - nonuniformity in gain from element to element (effective quantum efficiency and amplifier gain)
- spectral - nonuniformity in spectral response

The effect of streaking is the same as fixed pattern noise and it is highly objectionable in the image. If the sensor output is amplified and passed directly to a display, then solid-state imagers must possess highly uniform characteristics across the array. In some applications, compensation techniques may be used to remove streaking of the image.

REFERENCES


1. M.H. White, D.R. Lampe, F.C. Blaha, and I.A. Mack, "Characterization of Surface Channel CCD Imaging Arrays at Low Light Levels," IEEE Trans. J. Solid-State Circuits, SC-9, 1, 1974.

2. M.H. White and D.R. Lampe, "Noise Considerations in Solid-State Imagers," IEEE Intercon 74, New York City, N.Y., March 1974.

3. Optical Engineering Handbook, ed. J.A. Mouro, General Electric Co., Syracuse, N.Y., 1966.

4. Electro-Optics Handbook, RCA Defense Electronic Products, Burlington, Mass., 1968.

5. J.D. Plummer and J.D. Meindl, "MOS Electronics for a Portable Reading Aid for the Blind," IEEE J. Solid-State Circuits, SC-7, 111, 1972.

6. F.C. Eliot, "Geometric Design of Linear Array Detectors," IEEE Trans. Electron Devices, ED-21, 613, 1974.

7. M.H. Crowell and E.F. Labuda, "The Silicon Diode Array Camera Tube," B.S.T.J. 48, 1481, 1969.

8. W.B. Joyce and W.J. Bertram, "Linearized Dispersion Relation and Green's Function for Discrete Charge Transfer Devices with Incomplete Transfer," B.S.T.J. 50, 1741, 1971.

9. D.F. Barbe, "Imaging Devices Using the Charge-Coupled Concept," Proc. IEEE, 63, 38, 1975.

10. M.F. Tompsett, J. Vac. Sci. Technology, 9, 1166, 1972.